Moisture Sources and Sinks of Low-Level Jets in South China: A Backward and Forward Trace Model Approach

YUHAN LUO[a,b,c] AND YU DU[a,b,c]

[a] *School of Atmospheric Sciences, Sun Yat-sen University, and Southern Marine Science and Engineering Guangdong Laboratory (Zhuhai), Zhuhai, China*
[b] *Guangdong Province Key Laboratory for Climate Change and Natural Disaster Studies, Sun Yat-sen University, Zhuhai, China*
[c] *Key Laboratory of Tropical Atmosphere-Ocean System (Sun Yat-sen University), Ministry of Education, Zhuhai, China*

(Manuscript received 12 April 2024, in final form 3 April 2025, accepted 10 April 2025)

ABSTRACT: Low-level jets (LLJs) play a critical role as carriers of moisture, significantly influencing heavy rainfall. In South China, three distinct LLJ branches are identified: the boundary layer jets in the Beibu Gulf (BLJ-BG) and in the northern South China Sea (BLJ-SCS), as well as the synoptic-system-related LLJs in South China (SLLJ-SC). This study investigates their varying moisture transport, sources, and sinks utilizing the Hybrid Single-Particle Lagrangian Integrated Trajectory model (HYSPLIT), employing both backward and forward trace simulations. As the presummer rainy season progresses, the primary moisture sources of LLJs gradually shift southwestward from the South China Sea to the Indian Ocean. BLJ-BG predominantly directs moisture trajectories to cross the Indochina Peninsula, facilitating more moisture transport from the Indian Ocean (~42.7% after the onset of the South China Sea summer monsoon) and strengthening monsoonal moisture transport compared to non-BLJ-BG events. Conversely, BLJ-SCS consistently draws moisture from the South China Sea (~44.5%), with trajectories circumventing the Indochina Peninsula. Notably, BLJ-SCS transports even less moisture from the Indian Ocean than nonevent periods. After the monsoon onset, SLLJ-SC shares a common southwestern moisture channel with BLJ-BG and exhibits a pronounced tendency to transport moisture from the northern side (~10.3% moisture trajectories) compared to other LLJs, though still less than the non-SLLJ-SC events. Moisture transported by BLJ-BG (BLJ-SCS) is released in northeastern Guangxi (central Guangdong), coinciding with intensified inland maximum rainfall centers. SLLJ-SC transports more moisture further north into northern Jiangxi, aligning with the formation of rainbands further north.

SIGNIFICANCE STATEMENT: Different types of low-level jets (LLJs), including boundary layer jets and synoptic-weather-related LLJs occur frequently in South China during the presummer rainy season. This study distinguishes their respective roles in moisture transport from the perspectives of moisture paths, sources, and sinks. These LLJs do not uniformly enhance the southwesterly monsoonal moisture transport from distant oceanic regions. In particular, the boundary layer jets in the northern South China Sea predominantly draw moisture nearby. Moisture sinks associated with these LLJs align with areas where precipitation is intensified. This study provides valuable insights for forecasting extreme precipitation events in the region and establishes a connection between the origins and culmination of moisture in rainfall through the perspectives of LLJs as a crucial moisture carrier.

KEYWORDS: Precipitation; Mesoscale systems; Moisture/moisture budget

1. Introduction

Low-level jets (LLJs) are significant mesoscale phenomena occurring globally (Rife et al. 2010; Stensrud 1996). It is widely recognized that LLJs play a crucial role in influencing convection initiation, organization, maintenance, and propagation, consequently shaping horizontal distributions of rainfall (Du and Chen 2019a; Li and Du 2021; Monaghan et al. 2010). Generally, LLJs provide convergence at their termini and transport moisture and unstable energy, collectively enhancing precipitation (Du and Chen 2019b; Higgins et al. 1997; Luo and Du 2023; Trier and Parsons 1993).

In terms of moisture transport, LLJs are recognized as a major global mechanism, particularly in monsoonal regions (Algarra et al. 2019; Gimeno et al. 2016). For instance, Munday et al. (2021) identified that African LLJs transport the majority of water vapor to central Africa from the Indian Ocean based on vertically integrated water vapor flux. Montini et al. (2019) also employed this metric to illustrate how the increased moisture transport associated with South American LLJs contributes to enhanced precipitation over southeastern South America in recent decades. In the Indian monsoonal region, Xavier et al. (2018) found that moisture, as indicated by water vapor flux, brought by the strengthening of monsoon LLJs from the Arabian Sea is a necessary condition for heavy rainfall over the Indian subcontinent.

South China is significantly influenced by the complex Asian summer monsoon system, which encompasses both the South Asian and East Asian summer monsoons, with the latter extending to include the South China Sea summer monsoon (SCSSM) (Ding et al. 2004). LLJs occur frequently in this region and significantly affect precipitation during the presummer rainy season (Du and Chen 2019a; Liu et al. 2012;

Corresponding author: Yu Du, duyu7@mail.sysu.edu.cn

DOI: 10.1175/JCLI-D-24-0200.1

Liu et al. 2023; Zhang et al. 2024). Rainfall during this period, spanning from April to June and including before and after the onset of the SCSSM, contributes to approximately half of the annual precipitation (Luo et al. 2017). Additionally, LLJs can be typically classified into boundary layer jets (BLJs) and synoptic-system-related LLJs (SLLJs) based on their characteristics and formation mechanisms (Chen et al. 1994; Du et al. 2012, 2014). The BLJs typically occur below 1 km, located over the northern region of the South China Sea (SCS) (Dong et al. 2021; Du et al. 2022; Kong et al. 2020). The SLLJs with higher jet cores (~850 hPa) extend farther north, penetrating inland regions of South China (Du and Chen 2019a).

Both types of LLJs play distinct roles in influencing precipitation patterns in South China (Dong et al. 2021; Du et al. 2022; Du and Chen 2019a; Li and Du 2021; Du and Yi 2025; Su et al. 2025). Du and Chen (2019a) demonstrated that BLJs and SLLJs contribute to the net moisture fluxes in the boundary layer and more elevated layers, further influencing rainfall in the southern and northern regions of South China, respectively. Coastal BLJs exhibit two high-occurrence regions located in the Beibu Gulf and the northern SCS, respectively (Dong et al. 2021; Du et al. 2022). Dong et al. (2021) documented that the moisture transport, indicated by net moisture fluxes, associated with two BLJ branches contributes to the nocturnal and morning rainfall over Guangxi Province and Guangdong Province on the diurnal scale, respectively. Du et al. (2020) have illustrated marine BLJs over the northern SCS correlate with the low-level moistening through moisture budget diagnosis, further supporting the coastal convection initiation and the subsequent upscale convective growth. Previous studies have highlighted the distinct roles of LLJs in South China in moisture transport but have mainly utilized the Eulerian perspective and offered limited discussion on their moisture sources and regional contributions.

While the pathways and intensity of moisture transport can be calculated using the Eulerian method, the Lagrangian method excels in tracking moisture trajectories, providing clearer insight into the connections between evaporative origins and precipitation outcomes (Stohl and James 2004). From a Lagrangian perspective, recent studies have documented that moisture sources in South China shift with the onset of SCSSM in mid-May during the presummer rainy season by tracing air particles during precipitation events (Chen and Luo 2018; Chu et al. 2020; Peng et al. 2022; Xin et al. 2022). Primary moisture sources exhibit a transition from the SCS, Eurasian (EA) continent, and the western Pacific Ocean (WP) before the onset of SCSSM, to the Bay of Bengal, Indian Ocean, and the SCS after the onset.

Despite considerable progress in understanding moisture transport associated with precipitation, the detailed contributions of LLJs, as direct carriers in South China, remain underexplored. By mapping moisture sources and sinks of nocturnal LLJs globally, Algarra et al. (2019) documented that LLJs in South China associated with monsoonal flows transport more moisture from the Bay of Bengal and Indian Ocean to areas north of the LLJ cores compared to non-LLJ days. However, the diverse branches of LLJs in South China, including two branches of coastal BLJs and the inland branch of SLLJs, may play distinct roles in moisture transport and precipitation during the presummer rainy season. Therefore, several questions arise: 1) What are the quantitative differences in moisture sources of the three branches of LLJs in South China? 2) How is the moisture carried by LLJs related to precipitation patterns?

Accordingly, the objective of the present study is as follows: 1) to quantitatively examine the distinct moisture sources of three branches of LLJs in South China during the presummer rainy season utilizing the Hybrid Single-Particle Lagrangian Integrated Trajectory model (HYSPLIT) with backward trace simulations and 2) to establish a connection between the moisture transported by LLJs and precipitation patterns using the HYSPLIT model with forward trace simulations. The data and Lagrangian trace model are briefly introduced in section 2. Section 3 explores the moisture sources and sinks associated with LLJ events, and section 4 elaborates on the comparison of moisture sources and sinks between LLJ and non-LLJ events. The last section summarizes the findings and engages in a discussion.

2. Data and methodology

a. Data

The fifth major global reanalysis produced by the European Centre for Medium-Range Forecasts (ECMWF) (ERA5) data (Hersbach et al. 2020) with a horizontal resolution of $0.25° \times 0.25°$ and a time interval of 1 h is utilized for identifying LLJs and driving the HYSPLIT model. Additionally, the half-hourly gridded rainfall dataset produced by the Global Precipitation Measurement (GPM) Integrated Multisatellite Retrievals for GPM (IMERG) (Hou et al. 2014) with a $0.1° \times 0.1°$ spatial resolution is employed in this study to investigate precipitation associated with LLJs. The period used in the present study of ERA5 and IMERG spans from 2003 to 2022.

The definition of the SCSSM onset is based on the criteria established by the China National Climate Center, which require the persistent presence (more than two pentads) of westerlies and an equivalent potential temperature exceeding 340 K at 850 hPa within the SCS (10°–20°N, 110°–120°E). The intensity of the SCSSM is represented by the SCSSM index, which is calculated as the difference in the U-wind component at 850 hPa between two regions: (5°–15°N, 110°–120°E) and (20°–25°N, 110°–120°N) averaged over June.

b. Criteria for identifying LLJ and NLLJ events

Following the methodology of Du et al. (2022) and Du and Chen (2019a), LLJs are identified using two criteria based on hourly ERA5 data: 1) the maximum wind speed below 700 hPa exceeds 10 m s^{-1}, and 2) the wind speed decreases by at least 3 m s^{-1} from the wind speed maximum upward to the subsequent wind speed minimum at or below the 600-hPa level. LLJs, as defined above, are further classified into BLJs (maximum wind speed below 900 hPa) and SLLJs (maximum wind speed above 900 hPa).

Employing these criteria, the occurrence frequency of LLJs is calculated by dividing the total hours of BLJs and SLLJs by the total number of hours of the presummer rainy season from 2003 to 2022. The occurrence frequency of BLJs is observed to

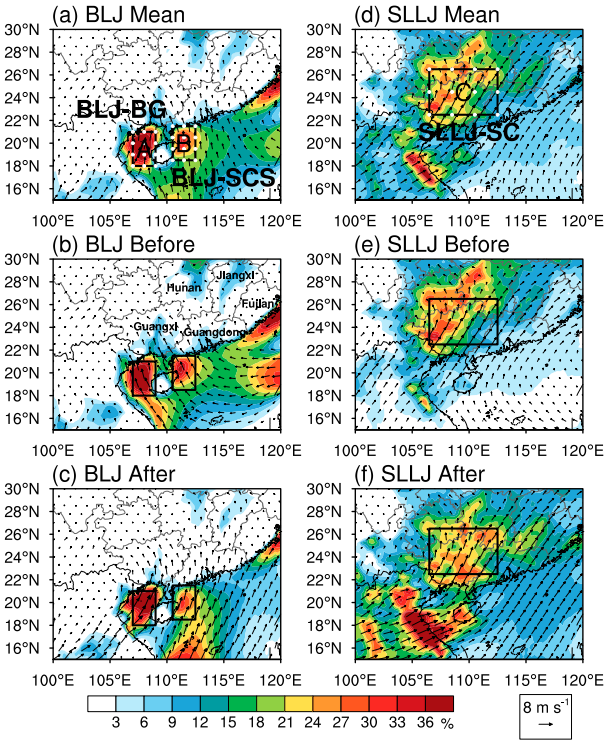

FIG. 1. Occurrence frequency distributions (shading; %) of (a)–(c) BLJs and (d)–(f) SLLJs, along with averaged horizontal winds (vectors) at (a)–(c) 950 hPa and (d)–(f) 850 hPa for (a),(d) seasonal mean, (b),(e) before, and (c),(f) after the onset of SCSSM. The black boxes A, B, and C indicate the regions selected for the BLJ-BG, the BLJ-SCS, and the SLLJ-SC events, respectively. The white dots in (a) and (d) denote the positions of releasing particles in the HYSPLIT model.

peak notably in the Beibu Gulf and the northern region of the SCS (Figs. 1a–c), consistent with Dong et al. (2021) and Du et al. (2022). In contrast, inland South China demonstrates a substantial peak in the occurrence frequency of SLLJs (Figs. 1d–f). Therefore, LLJ events are further categorized according to their high-occurrence regions. Events based on hourly data are designated as LLJ in the Beibu Gulf (BLJ-BG) and LLJ in the northern South China Sea (BLJ-SCS) events when over 50% of grid points within the Beibu Gulf (box A in Fig. 1a) and the northern SCS (box B in Fig. 1a) meet the established BLJ criteria, respectively. In the case of inland South China (box C in Fig. 1d), events with over 50% of grid points conforming to the SLLJ criteria are identified as SLLJ-SC events. Accordingly, non-LLJ (NLLJ) events are categorized into three types: NBLJ-BG, NBLJ-SCS, and NSLLJ-SC events. These NLLJ events correspond to scenarios when, within a 48-h period both before and after the given hour, the criteria for BLJ-BG, BLJ-SCS, or SLLJ-SC events are not met, respectively.

c. *HYSPLIT model and trajectories*

The HYSPLIT model (Stein et al. 2015), developed by the National Oceanic and Atmospheric Administration (NOAA) Air Resources Laboratory, Version 5.2, is utilized in the present study to track trajectories backward and forward. This model, operating within the Lagrangian framework, calculates the displacement of air particles based on averaged initial and first-guess wind velocity vectors in three dimensions (Draxler and Hess 1998). In backward mode, particles are traced back to their origins by releasing them into target areas, while in forward mode, they are projected from starting points to anticipate their future positions. The HYSPLIT model, renowned for its accuracy and reliability, has been extensively applied in quantitative research of moisture transport (e.g., Abel et al. 2022; Rapolaki et al. 2020; Zhang et al. 2021).

Particles are released into the atmosphere at the corresponding locations of LLJ events (white dots in Figs. 1a,d) and at altitudes matching the core of each LLJ type (500 m for BLJ events and 1500 m for SLLJ events). Additionally, the profiles of net water vapor fluxes show the strongest values at these altitudes, specifically at around 500 m for BLJ events and 1500 m for SLLJ events (not shown). These particles are then tracked backward for 240 h (10 days), aligning with the estimated duration of atmospheric moisture retention (Gimeno et al. 2021), to obtain trajectories of moisture transport leading to the LLJ events. Additionally, to investigate the destinations of moisture carried by LLJs, particles are tracked forward for 1 day after being released, considering the time lags between the LLJ peak (moisture convergence peak) and the precipitation peak (Luo and Du 2023; Xue et al. 2018). Trajectory outputs are generated hourly to leverage the high horizontal resolution of ERA5, finer than the distance a parcel would travel over the output interval at average wind speeds. Similarly, the methodology employed for tracing LLJ event trajectories is applied to non-LLJ events, with the tracking conducted at the specific times when these non-LLJ events occur.

The backward trajectories are further clustered using the Curve Clustering Toolbox (Gaffney 2004) to better reveal the variations in the water vapor paths, following Chen and Luo (2018) and Li et al. (2016). This clustering technique is adept at handling trajectories with varying durations, given that some particles may move beyond the model's vertical range up to 10 000 m, making it unable to track them for the full 240 h. Determination in the optimal number of clusters (k) is based on both the Monte Carlo cross-validated log-likelihood and predicted sum of squared errors (SSE). As the number of clusters grows, there is a notable rise in log-likelihood and a continuous reduction in SSE. Beyond a specific threshold, increasing k yields diminishing returns, indicating optimal cluster juncture (Gaffney et al. 2007).

d. *Calculation of moisture sources and sinks*

The HYSPLIT model tracks the trajectories of each released particle and calculates the corresponding specific humidity along these trajectories. From a Lagrangian perspective, the water vapor content of an air parcel changes due to processes like evaporation (actually refers to evapotranspiration including both transpiration and evaporation) from land and ocean surface into the air particles and precipitation processes that remove moisture from them. Therefore, the alterations of specific humidity reflect the net effect of these processes

(Shi et al. 2020; Stohl and James 2004). This relationship can be expressed as

$$e - p = m\frac{\Delta q}{\Delta t}, \tag{1}$$

where e and q represent the evaporation and precipitation, respectively, q is the specific humidity, and m is the mass of the air parcel. The change in specific humidity Δq at time t is calculated as

$$\Delta q_t = q_t - q_{t-\Delta t}, \tag{2}$$

where q_t represents the specific humidity at time t and $q_{t-\Delta t}$ represents the specific humidity at time $t - \Delta t$, with Δt being the 1-h interval of the trajectory output. When evaporation exceeds precipitation ($e - p > 0$), the air parcel gains water vapor, making the region a moisture source and resulting in an increase in q over time. Conversely, when precipitation surpasses evaporation ($e - p < 0$), the air parcel releases or loses water vapor, as water vapor condenses and precipitates out of the air parcel, rendering the region a moisture sink and leading to a decrease in q over time. By integrating the Δq over a 10- and 1-day period, moisture sources and sinks are identified, distinguished by regions with positive and negative values, respectively.

To quantitatively assess the contributions of various moisture origin regions, the "source attribution method" developed by Sodemann et al. (2008) is employed in the present study. The source attribution method has been widely adopted due to its incorporation of the effects from multiple cycles of moisture uptake and release (Chen and Luo 2018; Peng et al. 2022; Sun and Wang 2014; Zhang et al. 2021). This method tends to emphasize larger contributions from nearby regions. Regardless of using a method that does not reduce distant moisture contributions, the results are similar to the source attribution method (not shown). Following Zhang et al. (2021), during movement processes of the air parcel, when an air parcel absorbs water vapor from the source region ($\Delta q_t > 0$) and subsequently encounters a precipitation-dominated process at any subsequent time a after time t ($\Delta q_a < 0$), the effective moisture uptake is weighted as

$$\Delta q_{t^a} = \Delta q_t \times \frac{q_{a-\Delta t}}{q_a}, \tag{3}$$

where Δq_{t^a} represents the weighted Δq_t under the influence of moisture release at time a and $q_{a-\Delta t}$ and q_a denote the specific humidity at times $a - \Delta t$ and a, respectively. During the calculation of regional source contributions, Δq_t is considered zero when precipitation surpasses evaporation at time t ($\Delta q_t < 0$). The regional contribution ratio of moisture transport during movement processes (CR_m) is calculated by

$$\mathrm{CR}_m = \frac{\sum_1^n \Delta q_{t^{a,b,\ldots}}(i)}{\sum_1^m q_{-1}(i)}, \tag{4}$$

where $\sum_1^n \Delta q_{t^{a,b,\ldots}}(i)$ denotes the sum of effective moisture uptake by n trajectories passing through this region considering moisture release at times a, b,… after the time t and $\sum_1^m q_{-1}(i)$ represents the sum of the specific humidity recorded one hour before reaching the target areas for all m trajectories.

However, water vapor arriving at the target areas comprises two components: the variations in specific humidity along its trajectory during movement processes and the initial moisture content at the trajectory's origin. The initial humidity can influence the degree of subsequent variations in specific humidity during movement processes. For instance, higher initial humidity over oceans tends to result in less pronounced variations during movement processes. Additionally, the initial moisture content could contribute to water vapor arriving at destinations. Focusing solely on the contribution ratio of moisture changes along the trajectory could risk underestimating the effects of oceanic regions. Therefore, the contribution ratio of initial moisture (CR_i) is additionally calculated similarly with Eqs. (3) and (4) as

$$q_{t_0^a} = q_{t_0} \times \frac{q_{a-\Delta t}}{q_a}, \tag{5}$$

$$\mathrm{CR}_i = \frac{\sum_1^n q_{t_0^{a,b,\ldots}}(i)}{\sum_1^m q_{-1}(i)}, \tag{6}$$

where t_0 indicates the initial point of the backward trajectory.

3. Moisture sources and sinks associated with LLJ events

In this section, we examine the results derived from the HYSPLIT model concerning LLJ events. The analysis includes insights into moisture trajectories, the identification of moisture sources along these trajectories, and their quantitative regional contributions, as well as the determination of moisture sinks and their correlation with rainfall patterns.

BLJs and SLLJs are prominent features during the presummer rainy season in South China (Fig. 1). The direction of winds at 950 hPa in the coastal regions of South China shifts from southeasterly in the premonsoon period to southwesterly in the postmonsoon period (Figs. 1b,c). Conversely, at 850 hPa, the winds consistently maintain a southwesterly direction, with a noticeable intensification of southerly wind component before and after the onset of the SCSSM (Figs. 1e,f).

Figure 2 presents the relationship of the three branches of LLJs. The occurrence frequency of BLJ-BG events is approximately 30% during the presummer rainy season, with the higher frequency observed before the onset of the SCSSM. Similarly, BLJ-SCS events occur more frequently prior to the monsoon onset, but with lower frequency (~20%) compared to BLJ-BG events (Fig. 2a). In contrast, the occurrence frequency of SLLJ-SC is higher after the monsoon onset, but it remains lower than that of both BLJ-BG and BLJ-SCS. Figures 2b and 2c highlight the coexistence of BLJ-BG, BLJ-SCS, and SLLJ-SC events. The co-occurrence frequency of BLJ-BG and BLJ-SCS events is notably higher than the

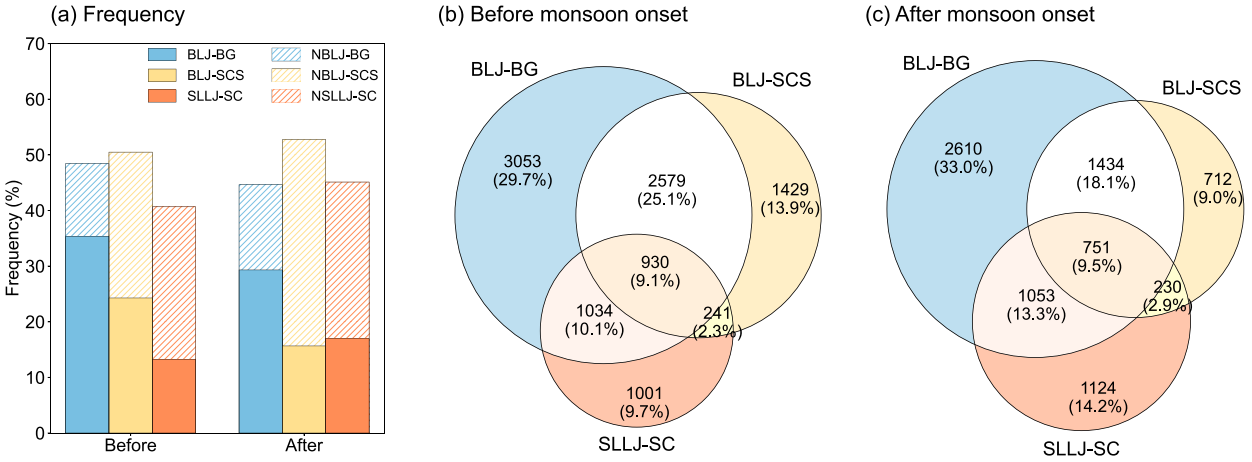

FIG. 2. (a) Temporal variation in LLJ and NLLJ event occurrence frequency and (b),(c) the number and ratio of BLJ-BG, BLJ-SCS, SLLJ-SC events, along with their co-occurrence relative to all events (b) before and (c) after the onset of the SCSSM. The circle sizes represent event counts.

occurrences of BLJ-SCS events alone, accounting for 34.2% and 27.6% of all LLJ events before and after the onset of the SCSSM, respectively. This result is consistent with findings by Du et al. (2022). After the monsoon onset, the coexistence of BLJ-BG and SLLJ-SC increases, constituting 22.8% of all LLJ events.

a. Moisture sources and their quantitative contributions

Figure 3 indicates terrain height as well as the distributions of trajectory frequency and their clusters for BLJ-BG, BLJ-SCS, and SLLJ-SC events. Optimal cluster numbers for each type of event are determined based on log-likelihood and SSE values, with four clusters identified for BLJ-BG events, five for BLJ-SCS events, and six for SLLJ-SC events (inset plots in Figs. 3b–d). The trajectories of these LLJ events predominantly originate from eastern Eurasia, the western Pacific Ocean, the SCS, and the Indian Ocean, aligning with previous studies on moisture sources of precipitation events and the SCSSM (Chen and Luo 2018; Peng et al. 2022; Shi et al. 2020; Li et al. 2019). The consistency is attributed to the significant impacts of LLJ events on rainfall patterns during the presummer rainy season and the close relationship with the dynamics of SCSSM.

For BLJ-BG events (Fig. 3b), the Indian Ocean acts as the predominant particle initial region, with over 50% of trajectories, including a longer distance group from the western Indian Ocean (24.25%) and a shorter length group from the middle of Indian Ocean (26.03%). Additionally, based on the trajectory frequency distribution, more than 0.5% of trajectories originate from the Southern Hemisphere crossing the equator. The western Pacific Ocean is another potentially important moisture source accounting for 34.89% of trajectories originating from this region. The northerly paths with 14.83% of trajectories originate from the midlatitudes of eastern Eurasia. Conversely, moisture paths in BLJ-SCS events (Fig. 3c) exhibit a more balanced distribution, with roughly equivalent numbers of moisture trajectories originating from the western Pacific Ocean, the SCS, and the Indian Ocean. In particular, the trajectories from the Indian Ocean tend to follow shorter paths in BLJ-SCS events, while BLJ-BG transports particles from more distant regions in the southwest to South China. BLJ-SCS features an additional cluster of trajectories originating from the East China Sea, accounting for approximately 12% of the total trajectories.

Trajectories in SLLJ-SC events (Fig. 3d) display a diverse pattern, with four clusters of moisture paths predominantly arriving from the southern periphery of South China. The trajectory frequency pattern, originating from the Indian Ocean in the southwest direction, shares similarities with BLJ-BG events. This pattern exhibits a tendency to pass over the Indochina Peninsula (ICP), with over 0.5% of trajectories originating from the Southern Hemisphere and traversing through the middle of the Indian Ocean. Notably, SLLJ-SC transports more trajectories from the inland of Eurasia, particularly along the southern edge of the Tibetan Plateau (14.18% of the trajectories), compared to the two coastal BLJ branches.

As the presummer rainy season progresses, there is a noticeable shift in moisture paths from Eurasia and the western Pacific Ocean toward the Indian Ocean (Fig. 4). This transition is closely related to the SCSSM evolution. However, each branch of LLJ events exhibits distinct variations in their associated moisture trajectories.

For BLJ-BG events, the majority of moisture trajectories before the onset of the SCSSM stem from the western Pacific Ocean, with more than 50% of the paths originating from this region (Fig. 4a). The proportion of moisture paths originating from the Indian Ocean exhibits a significant increase, rising from 17.05% to 92.42% with the onset of the SCSSM (Figs. 4a,b). Notably, BLJ-BG events tend to direct moisture trajectories passing over the Indochina Peninsula after the SCSSM onset (the inset plots in Fig. 4b).

BLJ-SCS events demonstrate a similar but milder shift in moisture paths, transitioning primarily from the southeast to the southwest of South China, with the proportion of the southwest

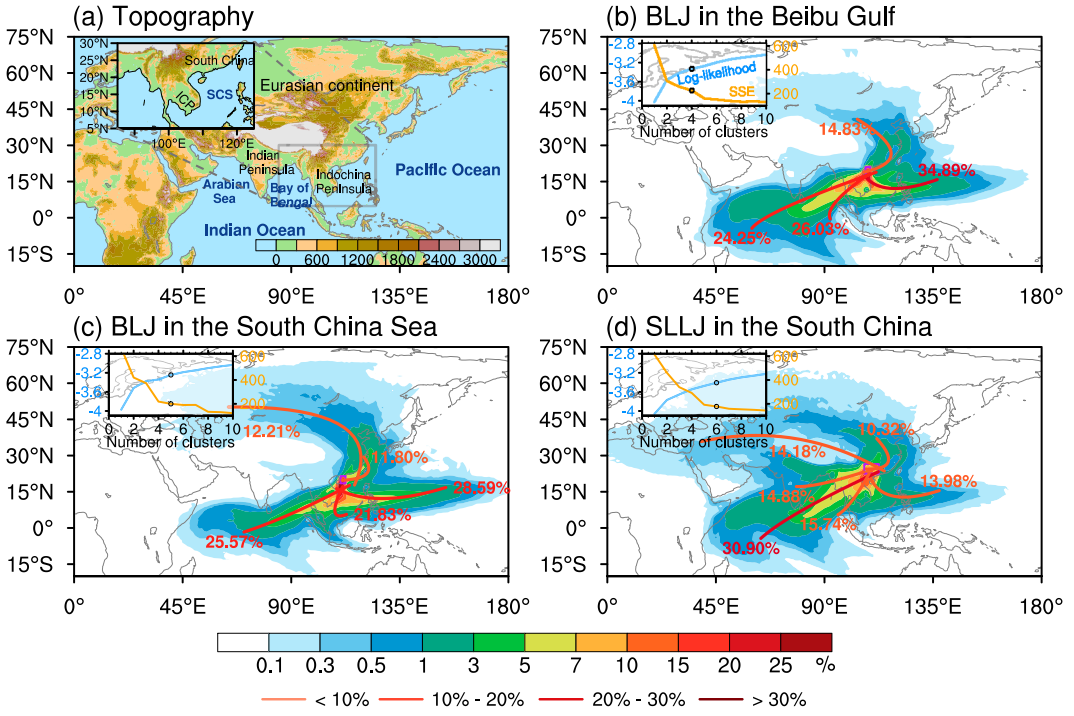

FIG. 3. (a) Terrain height (shading; m). Distributions of trajectory frequency (shading; %) for all (b) BLJ-BG, (c) BLJ-SCS, and (d) SLLJ-SC events. The orange-red lines and numbers illustrate clustered trajectories and their percentages of trajectory frequency. The purple boxes denote the regions of LLJ events. The inset plots in the top left corner indicate Monte Carlo cross-validated log-likelihood values (blue lines) and predicted SSE (orange lines) for various numbers of backward trajectory clusters. The black circles in the inset plots indicate the optimal number of clusters.

group increasing from 2.57% to 64.13% (Figs. 4c,d). Different from BLJ-BG events, trajectories of BLJ-SCS events tend to circumvent the Indochina Peninsula after the SCSSM onset (the inset plots in Fig. 4d).

For SLLJ-SC events, moisture paths exhibit a slightly different transition from two BLJ branches, shifting from the north to the southwest of South China (Figs. 4e,f). In particular, more trajectories accounting for 24.3% skirt the southern

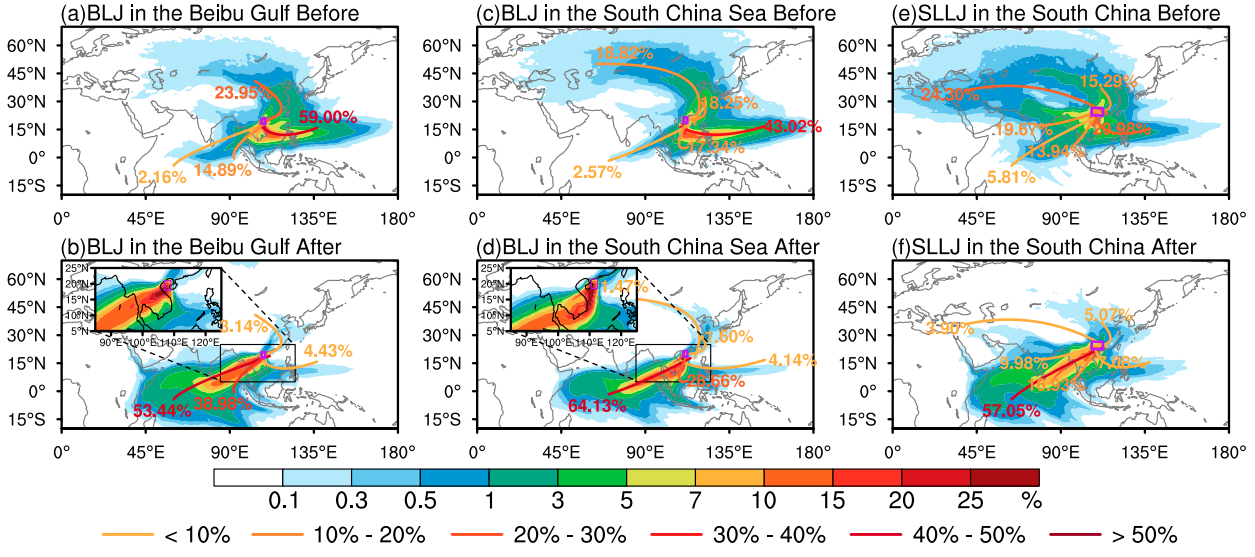

FIG. 4. Temporal evolution of trajectory frequency (shading; %) for (a),(b) BLJ-BG events, (c),(d) BLJ-SCS events, and (e),(f) SLLJ-SC events in (a),(c),(e) before and (b),(d),(f) after the SCSSM onset. The orange-red lines and associated numbers denote clustered trajectories and their ratios across various periods in Fig. 3. The inset plots in the top-left corner of (b) and (d) provide enlarged details near the ICP. The purple boxes denote the regions of LLJ events.

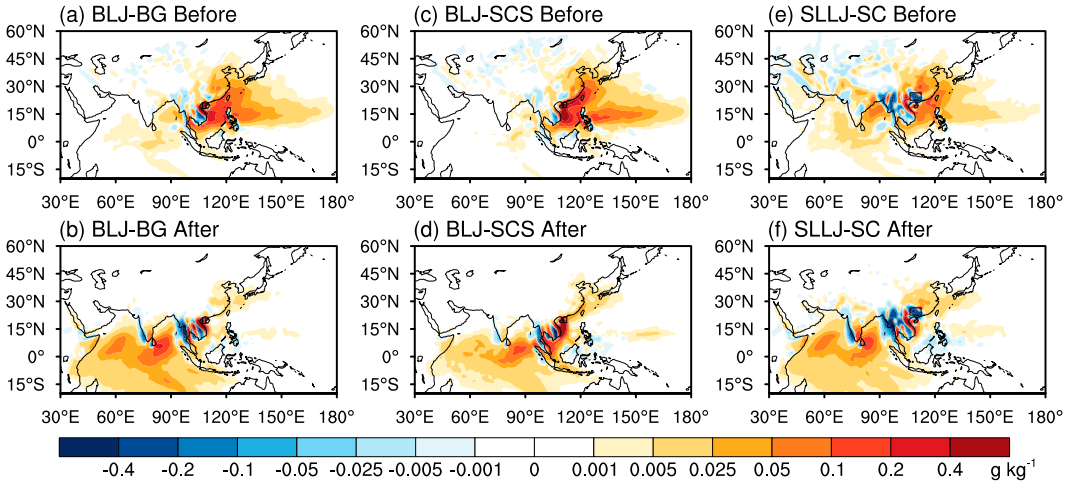

FIG. 5. Distributions of the event-averaged changes in specific humidity (evaporation minus precipitation) along trajectories (shading; g kg^{-1}) over 10 days of (a),(b) BLJ-BG events, (c),(d) BLJ-SCS events, and (e),(f) SLLJ-SC events in (a),(c),(e) before and (b),(d),(f) after the SCSSM onset. The black boxes denote regions of LLJ events.

edge of the Tibetan Plateau before the onset of the SCSSM, associated with the activities of the westerlies (Shi et al. 2020). Additionally, there is a notable increase in the proportion of moisture trajectories from the Bay of Bengal and the Indian Ocean, reaching about 80% after the SCSSM onset, while those from the southern edge of the Tibetan Plateau decrease substantially.

Figure 5 further depicts the changes in specific humidity (i.e., $e - p$) along the trajectories derived from the HYSPLIT model. The trajectories of LLJ events obtain abundant moisture from sources such as the western Pacific Ocean, the SCS, eastern China, the Bay of Bengal, and the Indian Ocean, where specific humidity increases or evaporation minus precipitation exceeds 0. Conversely, moisture depletion (moisture sinks with negative changes in specific humidity) along the trajectories primarily occurs over land or near topography, particularly on the Indian Peninsula and the Indochina Peninsula, where land precipitation consumes a portion of the moisture originating from distant oceans.

For BLJ-BG events, the variations in moisture sources closely track the progression of the SCSSM (Figs. 5a,b). Before its onset, moisture sources are predominantly distributed to the SCS followed by the western Pacific Ocean and the east coast of China (Fig. 5a). Under the prevailing southwesterly summer monsoon, BLJ-BG events mainly convey moisture from the Beibu Gulf and its southwest over the Bay of Bengal, the Arabian Sea, and the Indian Ocean with two centers in the middle of the Arabian Sea and near the Indian Peninsula (Fig. 5b).

A similar transition is observed during BLJ-SCS events, but with differences in detailed characteristics, particularly in the contribution of the SCS. BLJ-SCS transports more moisture from the distant western Pacific Ocean and the East China Sea before the SCSSM onset (Fig. 5c). However, significant increases in specific humidity, exceeding 0.4 g kg^{-1}, are consistently observed when trajectories pass over the northern region of the SCS. Circumventing the Indochina Peninsula prolongs the duration of obtaining water vapor on the SCS, making it a predominant moisture source. Additionally, the longer journey on the SCS shortens the distance deep into the Indian Ocean, with moisture source center over 0.2 g kg^{-1} closer to the Indochina Peninsula in the middle of the Bay of Bengal after the onset of the SCSSM (Fig. 5d) compared to BLJ-BG events (Fig. 5b).

The air parcels in SLLJ-SC events predominantly obtain moisture during movement processes from the east and north of South China as well as along the southern edge of the Tibetan Plateau from the coasts of the Arabian Sea and the Bay of Bengal, where air parcels undergo multiple cycles of graining and losing moisture along the trajectories before the SCSSM onset (Fig. 5e). With the procession of the SCSSM, the Arabian Sea and the Bay of Bengal become more significant moisture sources (Fig. 5f). In particular, moisture source pattern during SLLJ-SC events from the southwest direction is nearly identical to that of BLJ-BG events with two similar centers in the northern Indian Ocean but exhibits a slightly northern extension in SLLJ-SC events (Fig. 5f vs Fig. 5b).

Based on the horizontal distributions of changes in specific humidity, six important moisture source regions are divided for further quantitative investigation (Fig. 6a). The contributions of the moisture acquired both in the movement processes and at the initial time are considered, with their weights reduced when subsequent processes of moisture loss occur. In the oceanic regions such as the Indian Ocean, the SCS, and the western Pacific Ocean, initial moisture contributions are larger relative to land regions but are not as pivotal as those along the trajectories (Figs. 6b–d).

For BLJ-BG events, the SCS and the western Pacific Ocean are the predominant moisture source regions before the onset of the SCSSM, accounting for 33.1% and 26.5%, respectively (Fig. 6b). With the onset of the monsoon, there is a marked increase in contributions of the Indian Ocean, peaking at

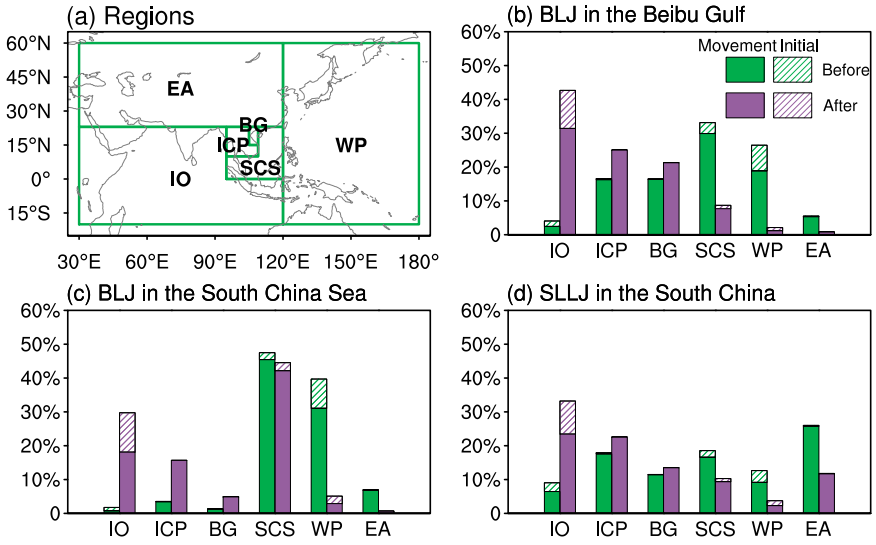

FIG. 6. (a) Distribution of six important moisture source regions, including the IO, the ICP, the BG, the SCS, the WP, and EA, and (b)–(d) quantitative contributions of these regions in (b) BLJ-BG, (c) BLJ-SCS, and (d) SLLJ-SC events before (green bars) and after (purple bars) SCSSM onset during the movement processes of air particles. The solid bars denote contributions of grained moisture during movement processes along the trajectories, while the shaded bars represent contributions of initial moisture.

42.7%, in contrast to the declines observed in the SCS and the western Pacific Ocean.

However, for BLJ-SCS events during the presummer rainy season, the SCS consistently delivers the highest percentage of moisture, exceeding 40% throughout the season, with a higher contribution occurring before the SCSSM onset (Fig. 6c). The trajectories from the southwest direction obtain water vapor primarily from the Indian Ocean, accounting for 29.7% of moisture after the monsoon onset, with its contributions showing a similar increasing trend but to a weaker degree compared to BLJ-BG events, whereas the contributions of the western Pacific Ocean exhibit a decreasing trend. The Indochina Peninsula and the Beibu Gulf contribute much less moisture than during BLJ-BG events due to the circumvention of the terrain on the Indochina Peninsula, resulting in fewer trajectories passing over the Indochina Peninsula during BLJ-SCS events.

Moisture derived from Eurasia notably contributes to SLLJ-SC events, particularly before the SCSSM onset, accounting for more than 25%, potentially due to their generation mechanisms (Fig. 6d). SLLJ-SC forms frequently in relation to synoptic forcing, such as low pressure anomalies and cold or stationary front (Du and Chen 2019a; Liu et al. 2020), facilitating interaction with cold air coming from the north. Moisture obtained from the Indian Ocean predominates under the monsoon background, constituting approximately 33%. Notably, the regional contributions from the southwest direction during SLLJ-SC events manifest nearly identical variations to those observed during BLJ-BG events after the SCSSM onset. Therefore, SLLJ-SC and BLJ-BG events may share a common moisture pathway from the southwest with the onset of the SCSSM.

Figure 7 reveals the interannual evolution of moisture contribution from the Indian Ocean (IO) and the SCS. For both BLJ-BG and BLJ-SCS events, the contribution from the IO shows a decreasing trend, while that from the SCS exhibits an increasing trend, though not significantly (below 90% significance level). The SCSSM index demonstrates a decreasing trend (Fig. 7a), suggesting a weakening of SCSSM (Wang et al. 2009). Interestingly, the correlation coefficient between the SCSSM index and the contributions of the IO (SCS) for BLJ-BG events is 0.738 (−0.567), both of which pass the 90% significance test. In contrast, for BLJ-SCS events, the correlations between the SCSSM index and contributions of IO and SCS are weaker, at 0.327 and −0.318, respectively. A stronger SCSSM is likely to result in greater moisture transport from the IO and less moisture transport from the SCS for BLJs, particularly for BLJ-BG. However, for SLLJ-SC, no significant trends are observed in the contributions from either the IO or the SCS (Figs. 7e,f), suggesting that the moisture transport in SLLJ-SC events may be influenced by factors beyond the SCSSM alone.

b. *Moisture sinks and their influence on rainfall*

LLJs significantly influence precipitation in South China through providing convergence at their termini, terrain-induced lifting, and moisture transport (Dong et al. 2021; Du et al. 2022; Du and Chen 2019a). Therefore, the distinct roles of moisture transport for each LLJ branch are discussed, as revealed by the destinations of the moisture carried by LLJ events and their potential impacts on precipitation. The analysis is facilitated through the application of the HYSPLIT model with forward trace simulations.

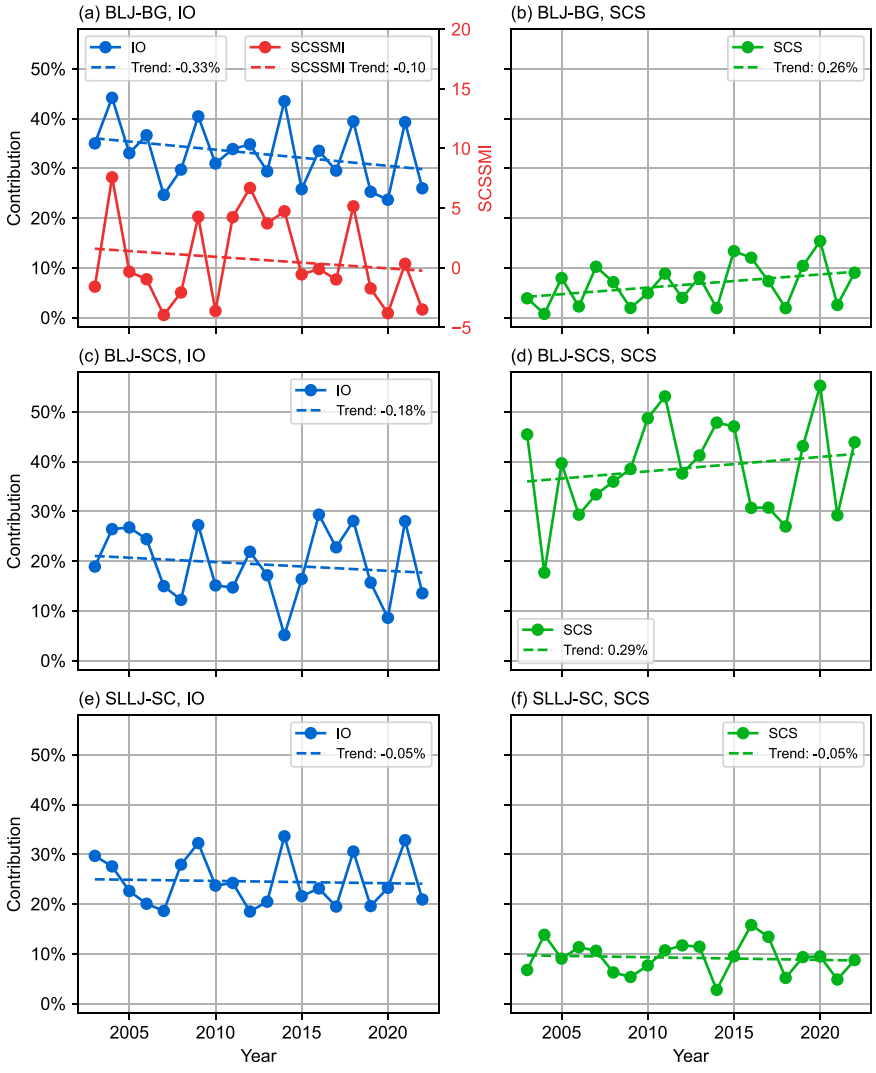

FIG. 7. Time series of regional contributions from the IO and the SCS for (a),(b) BLJ-BG, (c),(d) BLJ-SCS, and (e),(f) SLLJ-SC events after the onset of the SCSSM from 2003 to 2022. The red lines in (a) indicate the SCSSM index in June and its trend.

Figure 8a illustrates the climatological distribution of daily mean precipitation, featuring three main inland rainfall maximum centers (>10 mm day^{-1}) located in the northeastern Guangxi Province, central Guangdong Province, and northern Jiangxi Province, along with several coastal rainfall maximum centers, which is consistent with surface observations (Luo et al. 2017). The locations of moisture release correspond well with those primary inland rainfall regions across various branches of LLJ events.

For BLJ-BG events, moisture release accompanied with decreasing specific humidity over 1.8 g kg^{-1} predominantly occurs over northeastern Guangxi, along the windward slope of the Nanling Mountains (Fig. 8b). The topography of the mountains enhances orographic lifting and precipitation generation, resulting in rainfall exceeding 16 mm day^{-1}. The enhanced rainfall centers in central Guangdong and northern Jiangxi are also observed but with narrower spatial distributions and reduced intensities, potentially due to the coexistence of BLJ-SCS and SLLJ-SC events.

During BLJ-SCS events, southerly winds at 950 hPa are significantly strengthened in the northern SCS, with their termini located along the coast of South China (Fig. 8c). BLJ-SCS events facilitate heavier rainfall to surpass 18 mm day^{-1} in central Guangdong, corresponding well with the most significant moisture depletion exceeding 2.1 g kg^{-1}. Moisture release in BLJ-SCS events above 0.3 g kg^{-1} extends northward to Jiangxi, contributing to the northern rainband to a certain extent.

In SLLJ-SC events, southwesterly winds at 850 hPa undergo noticeable intensification compared to the seasonal mean wind field (Fig. 8d). The moisture carried by SLLJ-SC is mainly released in two key regions: a southern zone centered in northeastern Guangxi and a northern elongated band spanning northern Hunan, Jiangxi, and Fujian. The moisture

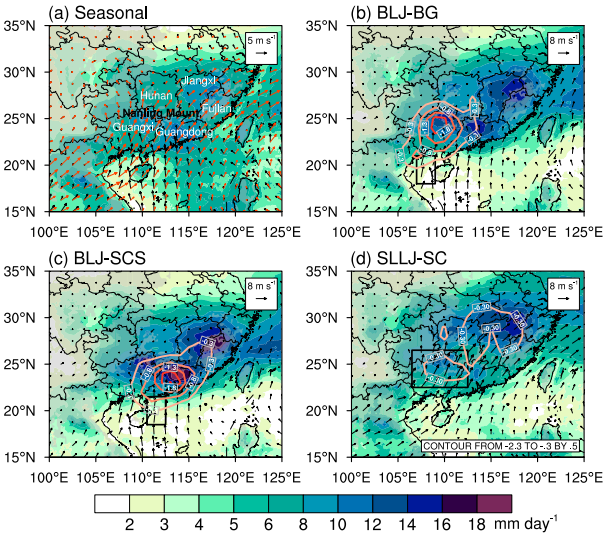

FIG. 8. (a) Distributions of seasonal mean daily precipitation (shading; mm day^{-1}) alongside wind vectors at 950 hPa (black) and 850 hPa (red). (b)–(d) Distributions of 24-h accumulated rainfall (shading; mm day^{-1}) and decreasing specific humidity output from the forward trace model (contours; interval: 0.5 g kg^{-1}) following (b) BLJ-BG, (c) BLJ-SCS, and (d) SLLJ-SC events. The wind vectors denote conditions at 950 hPa for BLJ-BG and BLJ-SCS events and at 850 hPa for SLLJ-SC events. The gray shadings indicate topography exceeding 500 m.

loss is relatively small at approximately 0.3 g kg^{-1} due to lower moisture content at higher levels. Correspondingly, two rainbands associated with SLLJ-SC events strongly correlate with the key regions of moisture release. In particular, the northern rainband, intensified to 18 mm day^{-1}, is positioned farther north compared to that observed in BLJ-BG and BLJ-SCS events and the seasonal mean.

4. Comparison between LLJ and NLLJ events

In this section, we compare the characteristics of moisture paths, sources, and sinks between LLJ and NLLJ events using similar backward and forward trace models. This comparison aims to distinguish the roles of the monsoonal background wind and highlight the distinct impacts of various branches of LLJs.

a. Differences in moisture paths

The moisture trajectories are generally more dispersed in NLLJ events, resulting in a more rational subdivision into multiple groups, specifically identified as five, five, and six groups for NBLJ-BG, NBLJ-SCS, and NSLLJ-SC events, respectively (Fig. 9).

For NBLJ-BG events, the horizontal distribution of moisture paths from various directions is relatively uniform, contrasting with a predominant influence from the south direction in BLJ-BG events (Fig. 9a vs Fig. 3b). An additional moisture cluster is identified during NBLJ-BG events, with 17.45% from midlatitude regions of Eurasia. Moisture paths from the northern regions account for more than 40% during NBLJ-BG events,

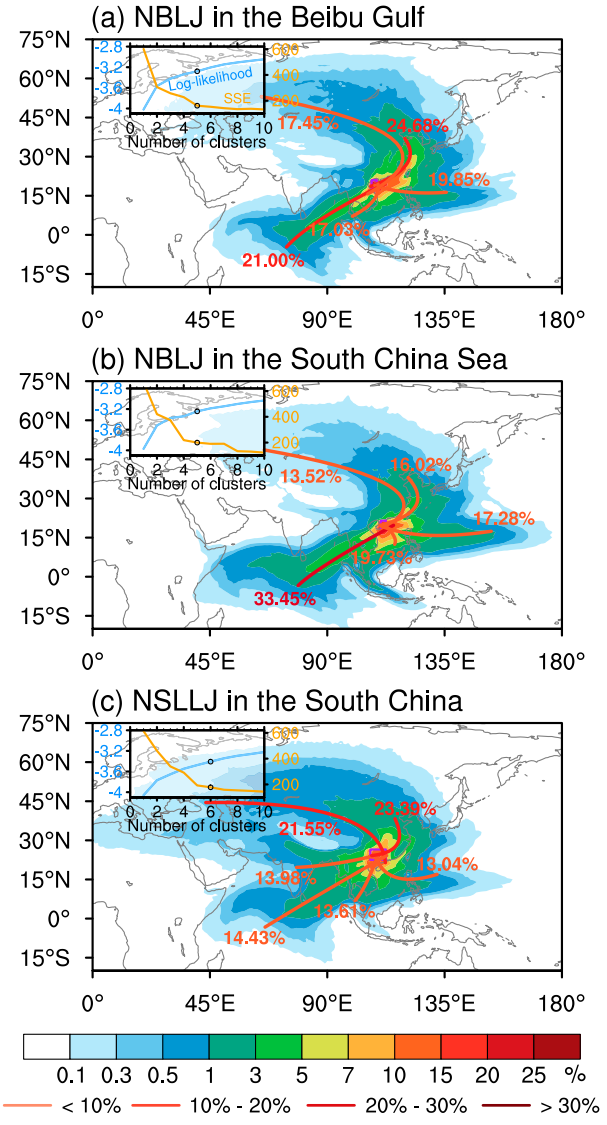

FIG. 9. As in Figs. 3b–d, but for (a) NBLJ-BG, (b) NBLJ-SCS, and (c) NSLLJ-SC events.

which is notably higher than BLJ-BG events (14.83%). Correspondingly, the proportion of moisture trajectories from the Indian Ocean and the western Pacific Ocean is lower than for BLJ-BG events, constituting about 38.03% and 19.85% during NBLJ-BG events, respectively. In contrast to BLJ-BG events with their trajectories extending to the distant Indian Ocean, NBLJ-BG events lack such extensive pathways, indicating a limited capacity to transport moisture over long distances from the south.

Surprisingly, for NBLJ-SCS events, there are more moisture trajectories originating from the Indian Ocean (~33.45%) surpassing the proportion of similar paths in BLJ-SCS events (~25.57%) (Fig. 9b vs Fig. 3c). These trajectories in NBLJ-BG events cover areas from the Southern Hemisphere and extend further southwest. Fewer and shorter trajectories originate from the SCS and the western Pacific Ocean during NBLJ-SCS events

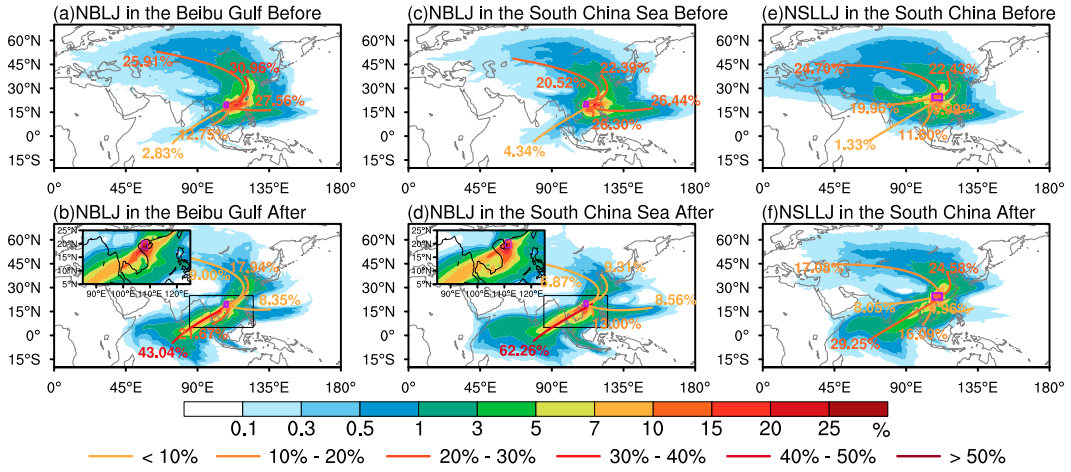

FIG. 10. As in Fig. 4, but for (a)–(b) NBLJ-BG, (c)–(d) NBLJ-SCS, and (e)–(f) NSLLJ-SC events.

compared to BLJ-SCS events, while more moisture paths are identified from the midlatitudes of Eurasia accounting for 29.54%, which is similar to the trajectory differences observed in BLJ-BG versus NBLJ-BG events.

The trajectory frequency distribution in NSLLJ-SC events exhibits a more dispersed pattern compared to SLLJ-SC events, especially over the Eurasian continent, despite clustering both into six groups (Fig. 9c vs Fig. 3d). Additionally, more than 40% of the trajectories originate from the midlatitudes of Eurasia and eastern China, subsequently entering South China from its northern direction. Two clusters originating from the southwest direction, including from the Indian Ocean (14.43%) and the southern SCS (13.61%), collectively constitute only less than 30% in NSLLJ-SC events. During NSLLJ-SC events, trajectories originating from the Southern Hemisphere in the middle Indian Ocean to South China comprise merely 0.1%, in contrast to over 0.5% observed in SLLJ-SC events according to trajectory frequency analysis.

Figure 10 illustrates the evolution of trajectories in NLLJ events. For NBLJ-BG events, water vapor trajectories, initially entering the Beibu Gulf from the east and north directions before the onset of the SCSSM, exhibit a transition to a predominantly southwest direction after the onset of the monsoon, aligning with the variations observed in BLJ-BG events (Figs. 10a,b vs Figs. 4a,b). This transition is primarily attributed to the procession of the SCSSM. However, it is noteworthy that the shift in NBLJ-BG events is milder, with the proportions of trajectories from the Indian Ocean increasing from 15.58% to 64.71% with the onset of the SCSSM. This is in contrast to a more pronounced change in BLJ-BG events, where the proportions increase from 17.05% to 92.42% during the same period. Correspondingly, moisture trajectories from the northern side exhibit an increase in NBLJ-BG events with 17.94% from eastern China after the onset of the SCSSM, relative to BLJ-BG events accounting for 3.14%.

The trajectory frequency distribution of NBLJ-SCS events exhibits a similar transition associated with the evolution of the SCSSM, which is interestingly as pronounced as that in BLJ-SCS events (Figs. 10c,d vs Figs. 4c,d). The trajectory pattern of NBLJ-SCS events before the onset of the SCSSM is similar to BLJ-SCS events except for larger ratios from the northern regions and fewer trajectories originating from the Indian Ocean in NBLJ-SCS events (Fig. 10c). In contrast, with the onset of the monsoon, similar proportion of moisture paths originate from the Indian Ocean extending over a greater distance during NBLJ-SCS events, accounting for 62.26%, compared to BLJ-SCS events (~64.13%) (Fig. 10d vs Fig. 4d). In particular, the trajectories during NBLJ-SCS events after the onset of the SCSSM, when encountering the Indochina Peninsula, show a preference to traverse the terrain instead of circumventing it as observed in BLJ-SCS events (inset plot in Fig. 10d).

Before the onset of the SCSSM, the trajectories in NSLLJ-SC and SLLJ-SC events exhibit similarities but a subtle difference in northern Africa with smaller frequency in NSLLJ-SC events (Fig. 10e vs Fig. 4e). With the progression of the SCSSM, the extent of trajectory frequency in NSLLJ-SC events covering the Indian Ocean increases yet remains smaller than those observed in SLLJ-SC events in each period (Fig. 10f vs Fig. 4f). In particular, the trajectory cluster originating from the Indian Ocean after the onset of the SCSSM for NSLLJ-SC events accounts for only 29.25% (more than 57% in SLLJ-SC events), and the trajectory frequency in the Bay of Bengal is approximately 8% (about 10% for SLLJ-SC events in Fig. 4f). Additionally, significantly higher proportions of trajectories from the northern regions exceed 40% of all trajectories after the onset of the monsoon for NSLLJ-SC events relative to SLLJ-SC events.

The potential mechanisms underlying the differences in trajectory frequency are further explored through large-scale circulations (Fig. 11). The primary distinction between LLJ and NLLJ is the presence of low pressure systems over land and the location of the subtropical high. Stronger low pressure systems, combined with the subtropical high located to the west, create a larger pressure gradient force that accelerates LLJs. These differences become more pronounced after the onset of the monsoon.

BLJs are characterized by prevailing southerly winds, while non-LLJs exhibit easterly winds prior to the monsoon onset,

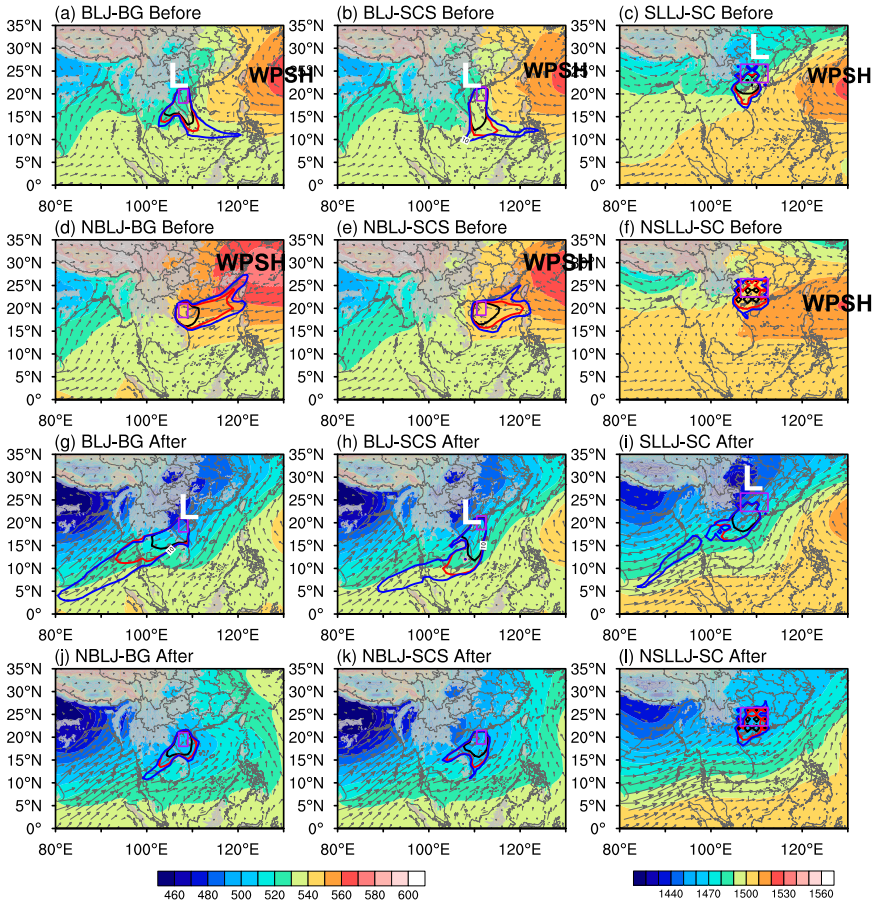

FIG. 11. The 24-h average geopotential heights (shadings; gpm) and wind vectors (left),(middle) at 950 hPa for BLJs events and (right) at 850 for SLLJ events (a)–(f) before and (g)–(l) after the onset of SCSSM. The black, red, and blue contours indicate the trajectory frequency exceeding 10% for −24, −72, and −240 h, respectively.

making the western Pacific Ocean a more important moisture source for non-LLJ events. After the monsoon onset, both types are dominated by southerly winds; however, the stronger wind speeds of LLJs enable them to transport moisture from more distant regions in a shorter period, effectively connecting to the stronger Indian monsoon and tracing moisture back to the Indian Ocean. In contrast, the weaker wind speeds in non-LLJ events limit the distance of moisture transport, resulting in a smaller contribution from the Indian Ocean, with a greater reliance on local sources such as the SCS.

Notably, moisture transport of BLJ-SCS exhibits a distinct pattern and this difference can be primarily attributed to their different formation mechanisms. Du et al. (2024) highlighted that the formation of BLJ-SCS is related to the horizontal momentum transport from jets located south of the Indochina Peninsula. As a result, when BLJ-SCS is traced backward, it generally moves southward, allowing moisture to remain over the SCS for a longer duration and thus reducing the relative contribution from the Indian Ocean.

In contrast, the southwestward transport of BLJ-BG can be interpreted in light of several dynamical mechanisms proposed in previous studies. These include the terrain-induced hydraulic jump effect along the Annamite Range in Vietnam (Kong et al. 2020) and the propagation of nocturnal LLJs, modulated by boundary layer inertial oscillations over the inland plains of the Indochina Peninsula, through terrain gaps in central Vietnam (Wang et al. 2022). Therefore, when traced backward, BLJ-BG tends to shift more toward the southwest, enhancing the background southwesterly flow of the SCSSM.

b. Differences in moisture sources

The moisture sources are further examined by comparing the event-averaged positive changes of specific humidity in LLJ events with those in NLLJ events (Fig. 12). Regions with positive values, indicated by reddish colors, are more active as moisture sources during LLJ events, while negative-value regions shown in bluish colors serve as more significant moisture sources during NLLJ events. Generally, both branches of BLJs primarily acquire more water vapor from the central and southern portions of the South China Sea, while SLLJ-SC transports more moisture originating from the western side.

Prior to the onset of the SCSSM, the most important moisture source regions with increasing specific humidity

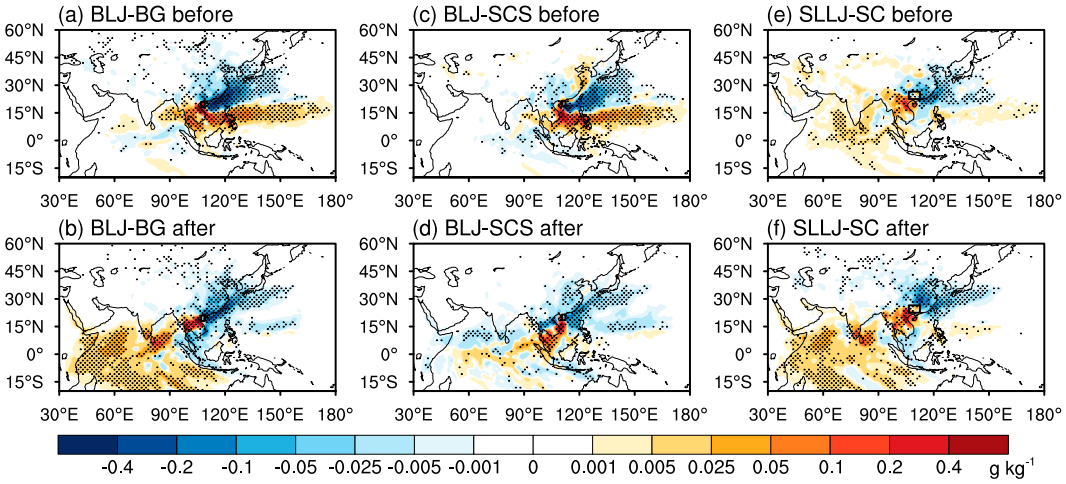

FIG. 12. Distributions of event-averaged differences in moisture sources (i.e., positive changes in specific humidity) (shading; g kg^{-1}) between (a),(b) BLJ-BG and NBLJ-BG events, (c),(d) BLJ-SCS and NBLJ-SCS events, and (e),(f) SLLJ-SC and NSLLJ-SC events (a),(c),(e) before and (b),(d),(f) after the SCSSM onset. The black boxes denote regions of LLJ events. The dots denote areas where the significance level of the differences exceeds 90% based on the two-tailed Welch's test.

exceeding 0.4 g kg^{-1} in BLJ-BG events include the western Pacific Ocean as well as the central and southern SCS (reddish colors), while their counterparts in NBLJ-BG events predominantly occur over the northern SCS and the East China Sea (bluish colors) (Fig. 12a). After the onset of the SCSSM, water vapor carried by BLJ-BG events is predominantly obtained from the western Indian Ocean and the Indochina Peninsula, whereas in NBLJ-BG events, it is acquired from closer locations to the target area, mainly distributed across the SCS and eastern China (Fig. 12b). Therefore, BLJ-BG significantly strengthen the monsoonal transport of water vapor from the distant oceanic regions, covering a broader area and exhibiting greater intensity compared to NBLJ-BG events.

In contrast, BLJ-SCS events are more effective in transporting water vapor from adjacent areas, with more moisture exceeding 0.4 g kg^{-1} over the SCS, compared to NBLJ-SCS events (Figs. 12c,d). Before the onset of the monsoon, while BLJ-SCS events also facilitate the transport of moisture from the distant oceanic regions relative to NBLJ-SCS events, the difference is of smaller magnitudes of approximately 0.1 g kg^{-1}. Correspondingly, less moisture transport from the northern side by NBLJ-SCS is associated with the progression of the monsoon. Conversely, trajectories in BLJ-SCS events acquire less moisture from the distant Indian Ocean after the onset of the SCSSM but more from the SCS, exhibiting a reverse trend compared to moisture transport of the monsoonal flows.

Trajectories along the southern edge of Tibetan Plateau obtain more moisture before the onset of the monsoon during SLLJ-SC events, while moisture sources located in Southeastern China and the East China Sea contribute more to NSLLJ-SC events (Fig. 12e). This phenomenon might be attributed to the formation of SLLJ-SC events in association with the low-level vortices or the southwest vortexes in South China (Du and Chen 2019a; Shen et al. 2020). The vortexes are related to lee side vortices, with circumvention of the topography on the southern side of the Tibetan Plateau being conducive to the development of these vortices (Wang and Tan 2014). In NSLLJ-SC events, moisture from the northern side, encompassing eastern China and the East China Sea, is significantly larger than SLLJ-SC events. There is a similar trend in NSLLJ-SC events with SLLJ-SC events where moisture from the southwest side becomes dominant with the progression of the SCSSM (not shown), despite a smaller magnitude (Fig. 12f).

The quantitative comparison of moisture contributions between LLJ and NLLJ events is exhibited in Fig. 13. In BLJ-BG events, the contributions of moisture originating from the southwestern direction, approximately 20% in the Indian Ocean, the Indochina Peninsula, and the Beibu Gulf, surpass those observed in NBLJ-BG events (approximately 15%) (Fig. 13a). The contribution of moisture from the Indochina Peninsula in BLJ-BG events exceeds 20%, partly due to its proximity to the Beibu Gulf, ensuring that the moisture obtained does not precipitate during transit. The SCS is the most important moisture source region in NBLJ-BG events, contributing 32.3% of the moisture.

There are slight but distinct differences in contribution between BLJ-SCS events and NBLJ-SCS events (Fig. 13b). In particular, the predominant moisture source region occurs in the SCS for both BLJ-SCS and NBLJ-SCS events, accounting for 46.3% and 41.3% of moisture, respectively, with a greater contribution in the former. The crucial role of BLJ-SCS events in moisture transport is to transport the water vapor from adjacent regions, resulting in slightly lower contributions of moisture from remote oceanic regions, including the Indian Ocean and the Pacific Ocean, compared to NBLJ-SCS events.

Conversely, apparent differences exist between SLLJ-SC and NSLLJ-SC events. In SLLJ-SC events, regions in the western side, such as the Indian Ocean and the Indochina Peninsula, serve as more significant moisture sources. Conversely, for NSLLJ-SC events, areas in the eastern side,

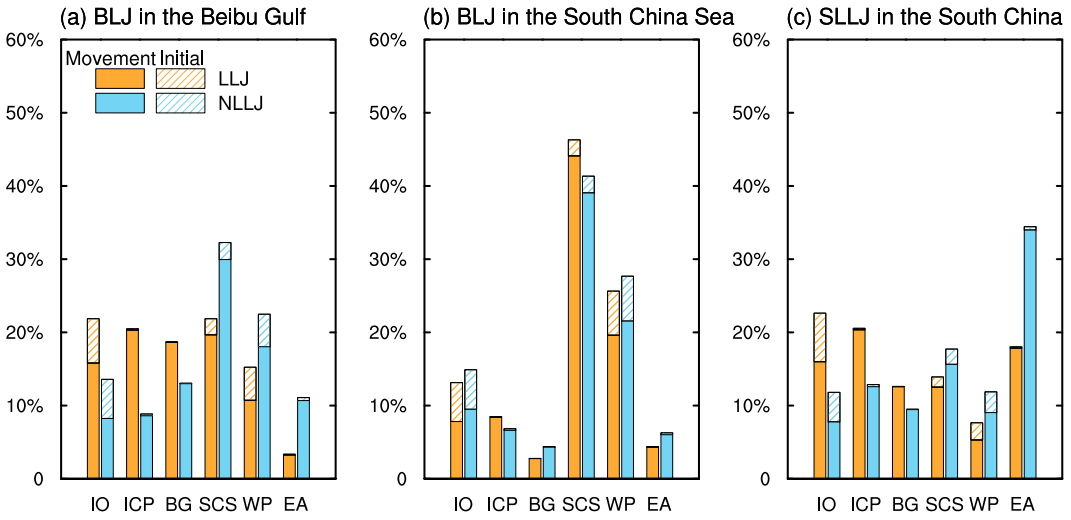

FIG. 13. Quantitative contributions of six important regions of moisture sources, as displayed in Fig. 6a, during the presummer rainy season for (a) BLJ-BG events, (b) BLJ-SCS events, and (c) SLLJ-SC events. The orange (blue) bars denote the contributions of LLJ (NLLJ) events. The solid (shaded) bars represent the contributions of grained moisture during movement (initial) processes.

including Eurasia and the western Pacific Ocean, contribute more to NSLLJ-SC events (Fig. 13c). Moisture obtained from Eurasia dominates, accounting for 34.4% in NSLLJ-SC events. In addition, the contributions of the moisture source regions in the southwestern direction for SLLJ-SC events exhibit a similar pattern to BLJ-BG events.

c. *Differences in moisture sinks and related precipitation*

In this section, we utilized a similar forward trace simulation to examine the differences in moisture release and the corresponding precipitation between LLJ and NLLJ events.

More significant moisture sinks are identified by reddish contours with negative values in LLJ events and by bluish contours with positive values during NLLJ events in Fig. 14. LLJ events promote inland rainfall, whereas precipitation following NLLJ events primarily occurs in the SCS.

Water vapor carried by NBLJ-BG events is primarily released northwest of the Beibu Gulf, resulting in a decrease in specific humidity by 0.7 g kg^{-1}, while considerable rainfall occurs over the SCS instead of the corresponding location of moisture release (Fig. 14a). Moisture transported by NBLJ-BG contributes little to rainfall patterns. The center of differences in moisture release in BLJ-BG events, exceeding 1.7 g kg^{-1}, and the corresponding maximum rainfall center are both located in northeastern Guangxi Province, blocked by the Nanling Mountain, consistent with Fig. 8.

In NBLJ-SCS events, approximately 0.2 g kg^{-1} more moisture contributes to rainfall in Hainan Island, with more rainfall exceeding 6 mm day^{-1} compared to BLJ-SCS events, and

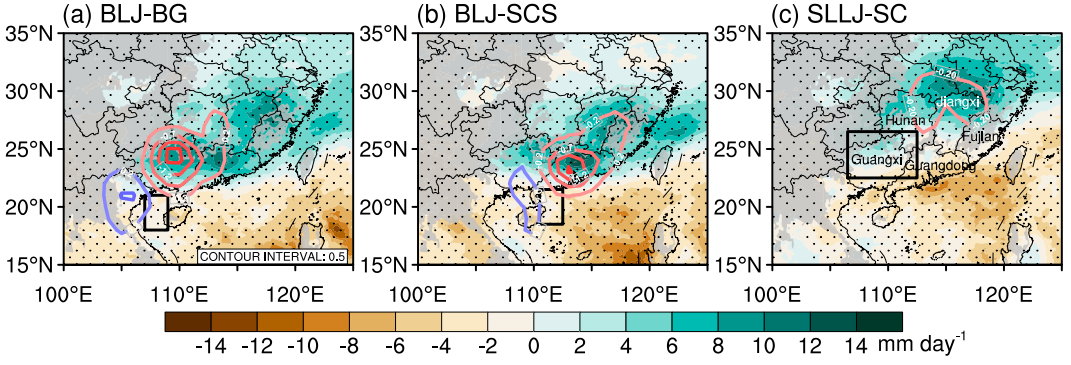

FIG. 14. Event-averaged differences in 24-h accumulated rainfall (shadings; mm day^{-1}) and decreasing specific humidity output from the forward trace model (contours; interval: 0.5 g kg^{-1}; red and blue contours indicate more active moisture sinks in LLJ and NLLJ events, respectively) between (a) BLJ-BG and NBLJ-BG, (b) BLJ-SCS and NBLJ-SCS, and (c) SLLJ-SC and NSLLJ-SC events. The gray shading represents topography over 500 m. The black boxes indicate regions of LLJ events. The dots denote areas with a significance level exceeding 90% based on the two-tailed Welch's test.

the coastal regions of the Beibu Gulf with a smaller augmentation (Fig. 14b). Nevertheless, more significant moisture release, decreasing by 1.7 g kg^{-1}, occurs in central Guangdong Province, resulting in precipitation exceeding 14 mm day^{-1} more than that observed in NBLJ-SCS events.

The intensified rainfall center in the northeastern Guangxi Province, which exceeds the seasonal mean during SLLJ-SC events, as well as the associated moisture release, is absent upon subtracting the effects of NSLLJ-SC events (Fig. 14c), suggesting insignificance of moisture transport by SLLJ-SC in this region. Accordingly, the intensified rainfall in the northeastern Guangxi Province during SLLJ-SC events might be attributed to the co-occurrence with BLJ branches. The moisture loss in northern Jiangxi Province during SLLJ-SC events exceeds that observed during NSLLJ-SC events by 0.2 g kg^{-1}, corresponding well with the heavier rainfall in SLLJ-SC events, while coastal rainfall is unrelated to the moisture transport of NSLLJ-SC, indicating the influence of other factors.

5. Summary and discussion

LLJs are significant meteorological phenomena for moisture transport, playing crucial roles in heavy rainfall events. In South China, three distinct branches of LLJs coexist: BLJ-BG, BLJ-SCS, and SLLJ-SC. This study investigates their moisture transport, sources, sinks, and associated rainfall by utilizing the HYSPLIT model with backward and forward trace capabilities.

Occasionally, three branches of LLJs occur concurrently. We examine their moisture sources and their regional quantitative contributions using the backward trace model and conduct a comparison with those in non-LLJ events. Under the monsoonal background wind, moisture paths gradually shift from the SCS to the Indian Ocean in the southwest direction with the progression of the SCSSM. However, each branch of LLJs exhibits unique characteristics.

In BLJ-BG events, the majority of moisture trajectories originate from the Indian Ocean and pass over the Indochina Peninsula, accounting for over 50% and peaking at 92.42% after the onset of the SCSSM. Similarly, in NBLJ-BG events, trajectories from the Indian Ocean dominate and peak after the monsoon onset with a lower proportion of approximately 64.71%. In contrast, moisture trajectories from the SCS and the Indian Ocean are comparable in BLJ-SCS events, with slightly more paths originating from the Indian Ocean, particularly after the onset of the SCSSM. In addition, moisture paths associated with BLJ-SCS events tend to circumvent the Indochina Peninsula, unlike BLJ-BG and NBLJ-SCS events. The trajectories of SLLJ-SC events are more concentrated on the southern side compared to NSLLJ-SC events which exhibit more evenly distributed trajectories across various directions.

The primary moisture sources are oceanic regions, including the East China Sea, the western Pacific Ocean, the SCS, and the Indian Ocean, followed by land regions over the Indochina Peninsula and Eurasia. Although the initial moisture contributions are greater over the ocean, they are overshadowed by those made during the transport along the trajectories. BLJ-BG events primarily obtain moisture from the South China Sea and the western Pacific Ocean before the onset of the SCSSM, while the Indian Ocean provides more than 40% of the moisture after the monsoon onset. Compared to NBLJ-BG events, BLJ-BG amplifies the moisture transport of the monsoonal flows from remote oceanic regions, covering a broader area and exhibiting greater intensity. The transition toward an increasing importance of the southwestern direction in moisture sources is detected in both BLJ-SCS and NBLJ-SCS events, with the latter showing a more pronounced shift. Nevertheless, the SCS consistently dominates moisture sources in BLJ-SCS events, contributing 46.3%, resulting in more moisture transport from adjacent regions and reduced contributions from other oceanic regions. For SLLJ-SC events, moisture obtained from the southwestern direction constitutes the largest proportion and exhibits similarities with that in BLJ-BG events, particularly after the monsoon onset, indicating that they share a common southwestern moisture channel after the onset of the SCSSM. Conversely, in NSLLJ-SC events, the Eurasian continent becomes the primary moisture source region. Overall, LLJs are more effective in transporting moisture from distant oceanic regions compared to NLLJs, with the exception of BLJ-SCS. However, LLJs are less effective in transporting moisture from East Asian land.

During LLJ events, precipitation is significantly enhanced, compared to the seasonal mean, with three primary land intensified rainfall centers located in northeastern Guangxi, central Guangdong, and northern Jiangxi. In contrast, during NLLJ events, rainfall mainly occurs over the SCS. Moisture carried by BLJ-BG events is released in northeastern Guangxi, coinciding with the intensified rainfall center, while moisture release in NBLJ-BG events primarily occurs south of Guangxi, not aligning with precipitation over the SCS. Similarly, moisture reduction along the trajectories identified in central Guangdong in BLJ-SCS events coincides with the enhanced rainfall center in that region. Moisture released in NBLJ-SCS events contributes to precipitation in Hainan Island and the northern Beibu Gulf. Compared to NSLLJ-SC events, SLLJ-SC transports more moisture further north to northern Jiangxi, contributing to the father northern rainbands.

This study deepens our understanding of the intricate moisture transport dynamics associated with different LLJ branches in South China, providing valuable insights for forecasting extreme precipitation events in the region. Previous studies have utilized the Lagrangian backward trajectory model by releasing particles at the time and location of precipitation events to investigate the moisture sources associated with rainfall. They indicated that the dominant moisture sources shift from the SCS before the onset of the SCSSM to the Bay of Bengal and the Indian Ocean in the southwest direction after the onset of the SCSSM (Chen and Luo 2018; Chu et al. 2020; Shi et al. 2020; Li et al. 2019). This study further reveals that moisture transport of LLJs in South China exhibits distinct characteristics rather than a uniform enhancement of monsoonal moisture transport. In particular, BLJ-SCS transports water vapor predominantly from the SCS, even after the onset of the monsoon, although the contribution from the Indian Ocean increases. The differences in moisture transport associated with various types of LLJs are highlighted, providing insights that would not be

obtained by solely tracing moisture based on precipitation in previous studies. In addition, this study establishes a connection between the origins of moisture and its culmination in rainfall through the perspectives of LLJs as a crucial moisture carrier. The results via the forward trace model confirm the contributions of moisture carried by LLJs in rainfall from the Lagrangian perspective.

Given that precipitation in South China is influenced by various factors such as cold pool, terrain, and coastline, and the particles are released at a single altitude level, the moisture release may explain part of the rainfall pattern. Moreover, since moisture fluxes are primarily concentrated at approximately 500 and 1500 m for BLJ and SLLJ events, the results of this study are representative of the majority of moisture sources. Sensitivity tests were conducted by releasing particles from three layers within the 400–600- and 1400–1600-m altitude ranges, instead of a single level. The results remain almost identical (not shown), confirming the robustness of the findings.

In the future, investigating the differences in moisture sources corresponding to whether precipitation occurs after LLJs would enhance our understanding of the impact of different moisture sources. Furthermore, the influence of moisture transport and sources on the detailed processes during convection, including convective initiation and development, needs to be explored in future research. In the context of global warming, according to the Clausius–Clapeyron (CC) equation, the water vapor content in the atmosphere is expected to increase, which may impact moisture transport. Additionally, changes in the intensity of the monsoon, oceanic evaporation, and precipitation processes are expected under global warming, and these complex interactions influencing LLJ moisture transport warrant further investigation in future studies.

Acknowledgments. This study was supported by the Guangdong Major Project of Basic and Applied Basic Research (Grant 2020B0301030004, 2024A1515510005, and 2025A1515011974), the National Natural Science Foundation of China (Grants 42475002), National Key Research and Development Program of China (2024YFC3013003), project supported by Southern Marine Science and Engineering Guangdong Laboratory (Zhuhai) (SML2024SP035, SML2023SP209, and 311024001), and the Key Innovation Team of the China Meteorological Administration (CMA2023ZD08). We also acknowledge the high-performance computing support from the School of Atmospheric Sciences of Sun Yat-sen University.

Data availability statement. The ERA5 reanalysis data are from ECMWF via https://cds.climate.copernicus.eu/cdsapp#!/dataset/reanalysis-era5-pressure-levels?tab=overview. The GPM-IMERG precipitation data are accessed via https://disc.gsfc.nasa.gov/datasets/GPM_3IMERGHH_07/summary. Version 5.3 of the HYSPLIT model used for backward and forward simulations in this study can be accessed at https://www.ready.noaa.gov/HYSPLIT.php.

REFERENCES

Abel, B. D., B. Rajagopalan, and A. J. Ray, 2022: Understanding the dominant moisture sources and pathways of summer precipitation in the Southeast Prairie Pothole Region. *Earth Space Sci.*, **9**, e2021EA001855, https://doi.org/10.1029/2021EA001855.

Algarra, I., J. Eiras-Barca, G. Miguez-Macho, R. Nieto, and L. Gimeno, 2019: On the assessment of the moisture transport by the Great Plains low-level jet. *Earth Syst. Dyn.*, **10**, 107–119, https://doi.org/10.5194/esd-10-107-2019.

Chen, Y., and Y. Luo, 2018: Analysis of paths and sources of moisture for the South China rainfall during the presummer rainy season of 1979–2014. *J. Meteor. Res.*, **32**, 744–757, https://doi.org/10.1007/s13351-018-8069-7.

Chen, Y.-L., X. A. Chen, and Y.-X. Zhang, 1994: A diagnostic study of the low-level jet during TAMEX IOP 5. *Mon. Wea. Rev.*, **122**, 2257–2284, https://doi.org/10.1175/1520-0493(1994)122<2257:ADSOTL>2.0.CO;2.

Chu, Q.-c., Q.-g. Wang, and G.-l. Feng, 2020: The roles of moisture transports in intraseasonal precipitation during the preflood season over South China. *Int. J. Climatol.*, **40**, 2239–2252, https://doi.org/10.1002/joc.6329.

Ding, Y., C. Li, and Y. Liu, 2004: Overview of the South China Sea Monsoon Experiment. *Adv. Atmos. Sci.*, **21**, 343–360, https://doi.org/10.1007/BF02915563.

Dong, F., X. Zhi, L. Zhang, and C. Ye, 2021: Diurnal variations of coastal boundary layer jets over the northern South China Sea and their impacts on diurnal cycle of rainfall over southern China during the early-summer rainy season. *Mon. Wea. Rev.*, **149**, 3341–3363, https://doi.org/10.1175/MWR-D-20-0292.1.

Draxler, R. R., and G. D. Hess, 1998: An overview of the HYSPLIT_4 modelling system for trajectories, dispersion, and deposition. *Aust. Meteor. Mag.*, **47**, 295–308.

Du, T., X. Zhi, Y. Wang, L. Zhou, L. Zhang, and S. Zhu, 2024: The distinct spatial patterns and physical mechanisms of coastal boundary layer jets over the northern South China Sea. *Mon. Wea. Rev.*, **152**, 2639–2660, https://doi.org/10.1175/MWR-D-23-0263.1.

Du, Y., and G. Chen, 2019a: Climatology of low-level jets and their impact on rainfall over southern China during the early-summer rainy season. *J. Climate*, **32**, 8813–8833, https://doi.org/10.1175/JCLI-D-19-0306.1.

——, and ——, 2019b: Heavy rainfall associated with double low-level jets over southern China. Part II: Convection initiation. *Mon. Wea. Rev.*, **147**, 543–565, https://doi.org/10.1175/MWR-D-18-0102.1.

——, and S. Yi, 2025: The relationship scenarios between boundary layer jet and coastal heavy rainfall during the pre-summer rainy season of South China. *J. Meteorol. Res.*, **39**, 26–40, https://doi.org/10.1007/s13351-025-4138-x.

——, Q. Zhang, Y. Ying, and Y. Yang, 2012: Characteristics of low-level jets in Shanghai during the 2008-2009 warm seasons as inferred from wind profiler radar data. *J. Meteor. Soc. Japan*, **90**, 891–903, https://doi.org/10.2151/jmsj.2012-603.

——, ——, Y.-l. Chen, Y. Zhao, and X. Wang, 2014: Numerical simulations of spatial distributions and diurnal variations of low-level jets in China during early summer. *J. Climate*, **27**, 5747–5767, https://doi.org/10.1175/JCLI-D-13-00571.1.

——, G. Chen, B. Han, C. Mai, L. Bai, and M. Li, 2020: Convection initiation and growth at the coast of South China. Part I: Effect of the marine boundary layer jet. *Mon. Wea. Rev.*, **148**, 3847–3869, https://doi.org/10.1175/MWR-D-20-0089.1.

——, Y. Shen, and G. Chen, 2022: Influence of coastal marine boundary layer jets on rainfall in South China. *Adv. Atmos. Sci.*, **39**, 782–801, https://doi.org/10.1007/s00376-021-1195-7.

Gaffney, S. J., 2004: Probabilistic curve-aligned clustering and prediction with mixture models. Ph.D. thesis, University of California, 281 pp.

——, A. W. Robertson, P. Smyth, S. J. Camargo, and M. Ghil, 2007: Probabilistic clustering of extratropical cyclones using regression mixture models. *Climate Dyn.*, **29**, 423–440, https://doi.org/10.1007/s00382-007-0235-z.

Gimeno, L., and Coauthors, 2016: Major mechanisms of atmospheric moisture transport and their role in extreme precipitation events. *Annu. Rev. Environ. Resour.*, **41**, 117–141, https://doi.org/10.1146/annurev-environ-110615-085558.

——, and Coauthors, 2021: The residence time of water vapour in the atmosphere. *Nat. Rev. Earth Environ.*, **2**, 558–569, https://doi.org/10.1038/s43017-021-00181-9.

Hersbach, H., and Coauthors, 2020: The ERA5 global reanalysis. *Quart. J. Roy. Meteor. Soc.*, **146**, 1999–2049, https://doi.org/10.1002/qj.3803.

Higgins, R. W., Y. Yao, E. S. Yarosh, J. E. Janowiak, and K. C. Mo, 1997: Influence of the Great Plains low-level jet on summertime precipitation and moisture transport over the central United States. *J. Climate*, **10**, 481–507, https://doi.org/10.1175/1520-0442(1997)010<0481:IOTGPL>2.0.CO;2.

Hou, A. Y., and Coauthors, 2014: The Global Precipitation Measurement mission. *Bull. Amer. Meteor. Soc.*, **95**, 701–722, https://doi.org/10.1175/BAMS-D-13-00164.1.

Kong, H., Q. Zhang, Y. Du, and F. Zhang, 2020: Characteristics of coastal low-level jets over Beibu Gulf, China, during the early warm season. *J. Geophys. Res. Atmos.*, **125**, e2019JD031918, https://doi.org/10.1029/2019JD031918.

Li, X., and Y. Du, 2021: Statistical relationships between two types of heavy rainfall and low-level jets in South China. *J. Climate*, **34**, 8549–8566, https://doi.org/10.1175/JCLI-D-21-0121.1.

——, W. Zhou, and Y. D. Chen, 2016: Detecting the origins of moisture over Southeast China: Seasonal variation and heavy rainfall. *Adv. Atmos. Sci.*, **33**, 319–329, https://doi.org/10.1007/s00376-015-4197-5.

Li, X.-f., Z.-h. Jiang, and Y. Shi, 2019: Moisture transport paths and sources of South China annually first rainy season and their relationship with the onset of the South China sea summer monsoon. *J. Trop. Meteor.*, **25**, 171–179, https://doi.org/10.16555/j.1006-8775.2019.02.004.

Liu, H.-B, L.-J Li, and B. Wang, 2012: Low-level jets over southeast China: The warm season climatology of the summer of 2003. *Atmos. Oceanic Sci. Lett.*, **5**, 394–400, https://doi.org/10.1080/16742834.2012.11447017.

Liu, X., Y. Luo, L. Huang, D.-L Zhang, and Z. Guan, 2020: Roles of double low-level jets in the generation of coexisting inland and coastal heavy rainfall over South China during the presummer rainy season. *J. Geophys. Res. Atmos.*, **125**, e2020JD032890, https://doi.org/10.1029/2020JD032890.

——, G. Chen, S. Zhang, and Y. Du, 2023: Formation of low-level jets over southern China in the mei-yu season. *Adv. Atmos. Sci.*, **40**, 1731–1748, https://doi.org/10.1007/s00376-023-2358-5.

Luo, Y., and Y. Du, 2023: The roles of low-level jets in "21·7" Henan extremely persistent heavy rainfall event. *Adv. Atmos. Sci.*, **40**, 350–373, https://doi.org/10.1007/s00376-022-2026-1.

——, and Coauthors, 2017: The Southern China Monsoon Rainfall Experiment (SCMREX). *Bull. Amer. Meteor. Soc.*, **98**, 999–1013, https://doi.org/10.1175/BAMS-D-15-00235.1.

Monaghan, A. J., D. L. Rife, J. O. Pinto, C. A. Davis, and J. R. Hannan, 2010: Global precipitation extremes associated with diurnally varying low-level jets. *J. Climate*, **23**, 5065–5084, https://doi.org/10.1175/2010JCLI3515.1.

Montini, T. L., C. Jones, and L. M. V. Carvalho, 2019: The South American low-level jet: A new climatology, variability, and changes. *J. Geophys. Res. Atmos.*, **124**, 1200–1218, https://doi.org/10.1029/2018JD029634.

Munday, C., R. Washington, and N. Hart, 2021: African low-level jets and their importance for water vapor transport and rainfall. *Geophys. Res. Lett.*, **48**, e2020GL090999, https://doi.org/10.1029/2020GL090999.

Peng, D., T. Zhou, Y. Sun, and A. Lin, 2022: Interannual variation in moisture sources for the first rainy season in South China estimated by the FLEXPART Model. *J. Climate*, **35**, 745–761, https://doi.org/10.1175/JCLI-D-21-0289.1.

Rapolaki, R. S., R. C. Blamey, J. C. Hermes, and C. J. C. Reason, 2020: Moisture sources associated with heavy rainfall over the Limpopo River Basin, southern Africa. *Climate Dyn.*, **55**, 1473–1487, https://doi.org/10.1007/s00382-020-05336-w.

Rife, D. L., J. O. Pinto, A. J. Monaghan, C. A. Davis, and J. R. Hannan, 2010: Global distribution and characteristics of diurnally varying low-level jets. *J. Climate*, **23**, 5041–5064, https://doi.org/10.1175/2010JCLI3514.1.

Shen, Y., Y. Du, and G. Chen, 2020: Ensemble sensitivity analysis of heavy rainfall associated with three MCSs coexisting over southern China. *J. Geophys. Res. Atmos.*, **125**, e2019JD031266, https://doi.org/10.1029/2019JD031266.

Shi, Y., Z. Jiang, Z. Liu, and L. Li, 2020: A Lagrangian analysis of water vapor sources and pathways for precipitation in East China in different stages of the East Asian summer monsoon. *J. Climate*, **33**, 977–992, https://doi.org/10.1175/JCLI-D-19-0089.1.

Sodemann, H., C. Schwierz, and H. Wernli, 2008: Interannual variability of Greenland winter precipitation sources: Lagrangian moisture diagnostic and North Atlantic Oscillation influence. *J. Geophys. Res.*, **113**, D03107, https://doi.org/10.1029/2007JD008503.

Stein, A. F., R. R. Draxler, G. D. Rolph, B. J. B. Stunder, M. D. Cohen, and F. Ngan, 2015: NOAA's HYSPLIT atmospheric transport and dispersion modeling system. *Bull. Amer. Meteor. Soc.*, **96**, 2059–2077, https://doi.org/10.1175/BAMS-D-14-00110.1.

Stensrud, D. J., 1996: Importance of low-level jets to climate: A review. *J. Climate*, **9**, 1698–1711, https://doi.org/10.1175/1520-0442(1996)009<1698:IOLLJT>2.0.CO;2.

Stohl, A., and P. James, 2004: A Lagrangian analysis of the atmospheric branch of the global water cycle. Part I: Method description, validation, and demonstration for the August 2002 flooding in central Europe. *J. Hydrometeor.*, **5**, 656–678, https://doi.org/10.1175/1525-7541(2004)005<0656:ALAOTA>2.0.CO;2.

Su, L., J. Hu, Y. Du, J. Li, and G. Chen, 2025: Boundary-layer and low-level moisture fluxes during low-level jet events in South China and their relationship with early summer rainfall. *J. Climate*, **38**, 1691–1713, https://doi.org/10.1175/JCLI-D-23-0561.1.

Su, B., and H. Wang, 2014: Moisture sources of semiarid grassland in China using the Lagrangian particle model FLEXPART. *J. Climate*, **27**, 2457–2474, https://doi.org/10.1175/JCLI-D-13-00517.1.

Trier, S. B., and D. B. Parsons, 1993: Evolution of environmental conditions preceding the development of a nocturnal mesoscale convective complex. *Mon. Wea. Rev.*, **121**, 1078–1098,

https://doi.org/10.1175/1520-0493(1993)121<1078:EOECPT>2.0.CO;2.

Wang, B., F. Huang, Z. Wu, J. Yang, X. Fu, and K. Kikuchi, 2009: Multi-scale climate variability of the South China Sea monsoon: A review. *Dyn. Atmos. Oceans*, **47**, 15–37, https://doi.org/10.1016/j.dynatmoce.2008.09.004.

Wang, Q.-W., and Z.-M. Tan, 2014: Multi-scale topographic control of southwest vortex formation in Tibetan Plateau region in an idealized simulation: Southwest vortex formation. *J. Geophys. Res. Atmos.*, **119**, 11 543–11 561, https://doi.org/10.1002/2014JD021898.

Wang, X., M. Xue, K. Zhu, Y. Zhang, and Z. Fan, 2022: Diurnal variation of summer monsoon season precipitation over southern Hainan Island, China: The role of boundary layer inertial oscillations over Indochina Peninsula. *J. Geophys. Res. Atmos.*, **127**, e2022JD037114, https://doi.org/10.1029/2022JD037114.

Xavier, A., A. Kottayil, K. Mohanakumar, and P. K. Xavier, 2018: The role of monsoon low-level jet in modulating heavy rainfall events. *Int. J. Climatol.*, **38**, e569–e576, https://doi.org/10.1002/joc.5390.

Xin, F., D. Peng, R. Liu, and S. C. Liu, 2022: Moisture sources for the weather pattern classified extreme precipitation in the first rainy season over South China. *Int. J. Climatol.*, **42**, 6027–6041, https://doi.org/10.1002/joc.7576.

Xue, M., X. Luo, K. Zhu, Z. Sun, and J. Fei, 2018: The controlling role of boundary layer inertial oscillations in Meiyu frontal precipitation and its diurnal cycles over China. *J. Geophys. Res. Atmos.*, **123**, 5090–5115, https://doi.org/10.1029/2018JD028368.

Zhang, S., B. Liu, G. Ren, T. Zhou, C. Jiang, S. Li, and B. Su, 2021: Moisture sources and paths associated with warm-season precipitation over the Sichuan Basin in southwestern China: Climatology and interannual variability. *J. Hydrol.*, **603**, 127019, https://doi.org/10.1016/j.jhydrol.2021.127019.

Zhang, X., Y. Luo, and Y. Du, 2024: Observation of boundary-layer jets in the northern South China Sea by a research vessel. *Remote Sens.*, **16**, 3872, https://doi.org/10.3390/rs16203872.